A robust optimised shunted electrodynamic metamaterial for multi-mode vibration control

Lawrence Singleton, Jordan Cheer, Steve Daley

[a]*Institute of Sound and Vibration Research, University of Southampton, University Road, Southampton, SO17 1BJ, Hampshire, UK*

Abstract

This paper presents a design approach for a shunted electrodynamic metamaterial (EDMM) for broadband robust vibration control. A unit cell of 12 inertial electrodynamic transducers is proposed, where the response of each transducer is tuneable via a connected resistive and inductive shunt circuit. The variations in the parameters of an off-the-shelf transducer are characterised experimentally, before the effect of this variation on the shunted response is investigated. It is shown that instability of the system is a limiting design factor. A problem is proposed whereby the resistive and inductive shunt values of an EDMM attached to a parametrically uncertain structure are to be found, and given the complexity of the design problem, a Particle Swarm Optimisation (PSO) is utilised to find a solution using an analytical model of the system. The results of the optimisation show that the effects of uncertainty in the actuators must be included, otherwise, the solution can be unstable. However, it is also shown that it is sufficient to ignore the uncertainty in the structure and optimise the EDMM considering actuator uncertainty alone, since the EDMM motion is then highly damped and, therefore, inherently robust to structural uncertainties.

Keywords:
vibration, metamaterial, optimisation, metaheuristics, electrodynamic

1. Introduction

The conservation of materials is becoming increasingly important, but as structural elements are made thinner and lighter, they also become more compliant and more receptive to vibration, which can lead to increased wear, or acoustic disturbance. Tuned Vibration Absorbers (TVAs) can achieve high levels of vibration attenuation [1], but multiple TVAs with resonance frequencies distributed around the target frequency are required to improve robustness to uncertainty in the target frequency [2]. For multiple target frequencies this means a large quantity of TVAs, and traditional TVAs are also often bulky or heavy, and therefore not suitable when there are weight or space constraints.

A potential solution to these vibration control challenges may be provided by metamaterials. Metamaterials consist of a number of periodically arranged sub-structures, which through local resonances or the interaction of scattered waves exhibit unusual properties, such as negative bulk modulus/stiffness and density/mass, at frequencies where the wavelength is long in comparison to the dimensions of the periodic structures they comprise of [3]. Elastic Metamaterials (EMMs) are a sub-category of these materials that are able to interact with elastic waves in solids. EMMs can be designed to interact with elastic waves in different ways, but the interest here focuses on their use as structural vibration absorbers [4, 5, 6, 7]. This can be achieved by using a locally resonant metamaterial, which consists of an array of small, resonant sub-structures with one or more degrees of freedom, and can be used to absorb vibration from a primary structure without significant additional mass. EMMs can be distributed over the surface of a structure, which means that unlike a TVA mounted at a single point on the structure, the same control force can be distributed over a much wider area. This means that they can potentially offer a better solution on thin, lightweight structures, where a control force applied to a single point would need to be constrained based on the structural strength.

Early examples of locally resonant EMMs demonstrated that a unit-cell containing mass-spring resonators exhibits frequency-dependent vibration absorption when the motion of the resonators cancels that of the structure [8, 9]. Similar to the approach taken in [2], multiple resonators in a unit cell, with tuning frequencies distributed around a target frequency have been shown to achieve greater absorption than if they were all tuned precisely to the target frequency [10]. This approach has also been extended to multiple target frequencies to achieve broadband attenuation, and also improve robustness to changes in the target frequency. However, this requires a large number of resonators tuned to different frequencies. This results in a complex design procedure, where the tuning frequencies and damping characteristics of the resonators must be carefully selected in order to keep the number of variously tuned resonators within practical manufacturing and installation limitations.

To be able to effectively design a passive EMM with multiple tuning frequencies requires a highly refined model of the EMM in order to predict its behaviour, but would also likely still require multiple prototyping runs to fine tune the design. Furthermore, once built, the tuning frequencies and damping characteristics cannot be changed. An alternative approach is to use tuneable resonators. One way of realising this would be by connecting resonant electronic impedance circuits to a proof mass electromechanical transducer, a technique known as shunting [11]. Shunting has the benefit over other methods of variable tuning, such as mechanically variable stiffnesses, of being easily translatable to a small scale for integration into a metamaterial.

The use of shunted electrodynamic assemblies as vibration absorbers has already been explored in a number of studies [12, 13, 14], but the effect of parametric uncertainty or variability in the electromechanical response of the transducers, on the efficacy of a proposed tuning approach, has not yet been considered in the literature, which has generally only considered a small number of devices of known parameters. However, in a fixed system, variation in the electrodynamic transducers will affect the shunted response and with impedances where the real or imaginary part is negative, under certain conditions may in fact result in instability. Self-tuning control strategies such as those demonstrated in [15] are able to avoid this, but require a variable shunt impedance which is only achievable using a digital synthetic impedance. Digital synthetic impedances introduce further complexities due to latency, and require high speed, high sample-rate converters and additional circuitry in addition to any controller [16]. In the case of using an array of shunted electrodynamic transducers to realise a metamaterial, it will not be practicable to characterise each transducer in advance and it will likely be necessary to utilise low-cost, small inertial transducers, which although readily available [17, 18], have a specified variability in their parameters of up to 10%. Reducing manufacturing tolerances increases production cost, and measuring individual responses is unlikely to be practical for large arrays. Therefore, it is important to consider this uncertainty in the design of the metamaterial.

This paper proposes a tuned-shunt electrodynamic metamaterial (EDMM) and a design procedure for the robust absorption of multiple modes of structural vibration in the presence of structural uncertainties. The novel multi-resonator unit cell consists of a number of inertial electrodynamic transducers, tuned independently via a fixed shunt impedance. Existing studies utilising tuned electrodynamic transducers as vibration absorbers have investigated using a relatively small number of devices with known characteristics. This study investigates the potential for much larger numbers of these devices to be used, with realistic uncertainties in the device characteristics, where it may not be practicable to measure each transducer individually, and without using adaptive controllers. In order to take into account the uncertainties, the distribution of variation in the parameters of an electrodynamic transducer is characterised experimentally, and these realistic distributions are used to quantify the robustness during the optimisation process. The component values of a resistive and inductive shunt are optimised directly using a Particle Swarm Optimisation (PSO) algorithm. The following sections set out the EDMM design, before demonstrating the principles of tuning, and the effect of different impedances on the dynamic response and system stability. The parametric variation in the miniature electrodynamic transducers is then characterised, and the effect of this variation investigated. An analytical model of a vibrating structure with an attached EDMM is then described, and finally the procedure and results of an optimisation study used to select the impedances of a multi-resonator EDMM unit cell is set out.

2. A Shunted Electrodynamic Metamaterial

This paper proposes a novel shunted electrodynamic metamaterial (EDMM) for the robust absorption of multiple modes of vibration. This EDMM consists of multiple, differently-tuned resonators in a unit cell to achieve multi-mode control that is robust to variations in the structure and uncertainty in the electrodynamic transducers. A specific example is considered here, where a unit cell of 12 resonators is proposed for the control of 3 adjacent modes of an attached structure, which will be described in Section 4, with each resonator tuned individually and the unit cell repeated periodically over the structure, as shown in Figure 1. This is seen as a practical compromise between the ability to achieve a robust distribution of tuning frequencies, whilst also keeping the size of the unit cell to a minimum so that it is small compared to the wavelength of vibration.

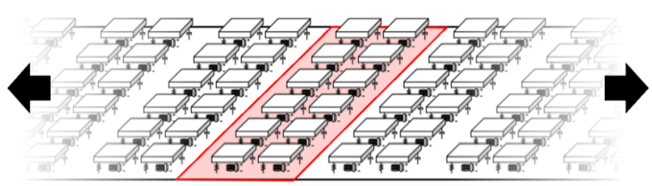

Figure 1: EDMM concept with the unit cell of 12 resonators highlighted in red, and repeated along the structure.

The tuning of the response of an individual electrodynamic transducer is achieved by connecting a shunt impedance across its electrical terminals, which can have positive or negative components. Modelling the transducer as a SDOF mass-spring-damper, Figure 2 shows the electromechanical and mechanical-only equivalent models of an RL shunted inertial electrodynamic transducer with: moving mass, m_r; suspension stiffness, k_r; damping coefficient, b_r; voice coil inductance, L_e; voice coil resistance, R_e; transduction coefficient, Bl; shunt inductance, L_s; and shunt resistance, R_s. j is the imaginary unit where $j = \sqrt{-1}$, and ω is the circular frequency. The shunt impedance acts as an additional effective mechanical impedance, operating in parallel to the suspension stiffness and damping, and can be designed to modify the resonance frequency and damping of the transducer. As a negative impedance requires power to reverse the current flow, it is an active component, and therefore can result in instabilities, which will need to be considered in the design of the proposed shunted EDMM.

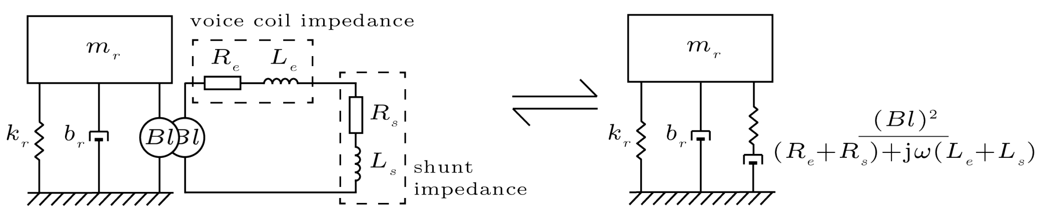

Figure 2: Left: Electro-mechanical diagram of an transducer with voice coil impedance of $R_e + j\omega L_e$ and series resistor-inductor (RL) shunt impedance of $R_s + j\omega L_s$. Right - mechanical-only equivalent of the shunted transducer.

With a large number of transducers, accurate measurement of the response of each individual device is unlikely to be practical, and in-fact the response may change over time due to suspension run-in/creep, temperature, or degradation, for example. The selection of shunt components to tune the response is highly reliant on the accuracy of the modelled transducer response, and producing transducers with high manufacturing tolerances to minimise this variation is very costly. However, by taking into account the transducer uncertainties in the shunt design process, the costs of the proposed EDMM can be minimised by enabling the use of mass-produced transducers, with relatively poor tolerances. Although uncertainty in the shunt circuit itself may well be present, it is considered that high quality components have a much smaller tolerance relative to the transducers that will be considered, and are still relatively low cost. Therefore, this study does not take uncertainty in the shunt circuit into account.

The Tectonic Audio Labs TEAX09C005-8 miniature inertial actuator [17] (shown in Figure 3) is selected to be used in this study. Since this is a low-cost, off-the-shelf device, it is well suited for implementation in the large numbers required for the proposed design, shown in Figure 1. It also presents a practical level of variability that might be expected of a device that is produced in high volumes, and therefore facilitates a realistic investigation into the effects of uncertainties. In the following sections, the effect of different positive and negative shunt impedances on this transducer will be investigated, and the system stability will be analysed.

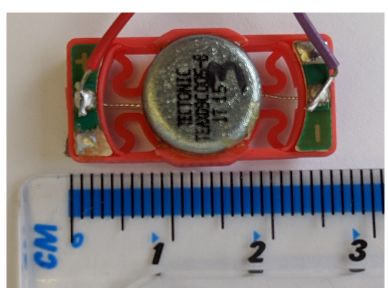

Figure 3: Tectonic Audio Labs TEAX09C005-8.

2.1. *The effect of shunt impedance on an electrodynamic transducer*

The effect of a shunt impedance on the response of an electrodynamic transducer can be evaluated by modelling the inertial transducer as a SDOF mass-spring-damper, with the addition of an electromechanical transduction mechanism between the mass and the base, in parallel with the suspension. In an open circuit with the voice coil un-terminated, the effect of the magnet and coil can be disregarded, however, with the voice coil shorted or shunted, the back electromotive force (EMF) transduced when there is a net velocity difference between the base and the mass, presents an additional impedance to motion. The effective mechanical impedance of the electrical part, Z_{me}, is related to the total electrical impedance of the closed loop, Z_{es}, by [13]

$$Z_{me} = j\omega \frac{(Bl)^2}{Z_{es}}, \tag{1}$$

where Bl is the transduction coefficient, or 'force factor' equal to the magnetic flux density, B, multiplied by the length of the coil, l. A resistor-inductor (RL) shunt circuit has been demonstrated in [14] to effectively tune the resonance frequency of an electrodynamic transducer, and therefore, the same approach is used in this study. The shunted transducer is therefore approximated by the SDOF model already set out in Figure 2.

The study presented in [14] uses large, proof-mass transducers with a natural frequency at the lowest bound of the tuning range, and therefore only considers the case where the resonance frequency of the transducer is increased by the shunt, which does not require the system to have an overall negative impedance, and therefore avoids the risk of instability. However, the proposed EDMM requires resonators with a small mass, and from a practical standpoint, small form-factor and low-cost. Transducers meeting these requirements with a low resonance frequency are not readily available, and so it is proposed here that if the resonance frequency of the transducer can also be decreased using negative inductances, this would allow the use of more readily available, lower-mass devices with higher natural frequencies. A total loop impedance with a resistive and inductive component presents a complex mechanical equivalent, and the equation of motion of the system becomes fourth-order. This means that the required values of R_s and L_s cannot be calculated straightforwardly from the desired resonance frequency and damping ratio. In the study presented in [14], although the effect of varying the shunt resistance and inductance is considered, for the time-varying sweep in order to easily tune the resonance frequency a fixed resistance is used to completely cancel the coil resistance and the inductance only is used to sweep the resonance frequency and damping ratio across a range. By cancelling the resistance of the circuit completely using a negative resistance equal to the coil resistance, the shunt presents an effective stiffness determined by the inductive components only, which is then proportional to the square of the resonance frequency, and the device can be easily tuned to a specified frequency. However, in the presence of transducer uncertainty, perfect cancellation of the coil resistance is not guaranteed, and the circuit resistance can be utilised to modify the damping of the transducer as well. Therefore, it is beneficial to consider both shunt component values in the tuning process. To demonstrate this, Figure 4 shows how the impedance of the transducer base to displacement varies when the transducer is shunted with different resistance and inductance values. For reference, the solid line in 4 shows the open-circuit impedance of the transducer. If the total electrical impedance is set equal to either a negative (– – –) or positive (—□—) inductance only, the resonance frequency is shown to decrease or increase respectively, but with no visible change in the damping. However, if the total electrical impedance also has a negative resistance component in each case (– - – - and · · · · · ·), it can be seen how the damping of the transducer is reduced, but the frequency tuning effect of the inductor is also reduced. Therefore, any design procedure must consider both parameters simultaneously to ensure that both the tuning frequency and damping are as specified. It also leads us to a hypothesis that uncertainty in the resistance of the coil, R_e, is likely to result in both a change in damping and a shift in tuning frequency, which could significantly impact the efficacy of the EDMM, and needs further investigation.

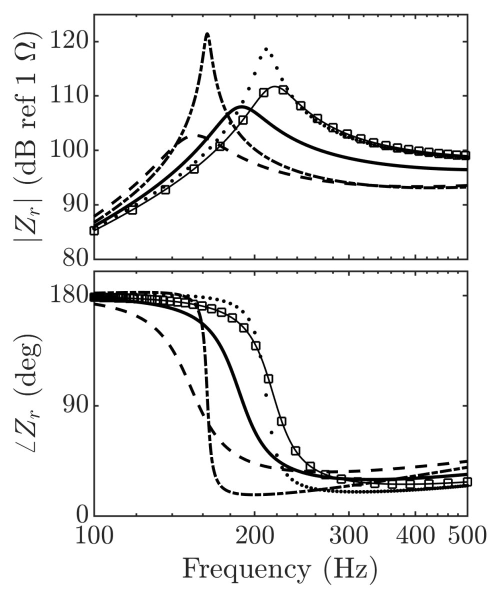

Figure 4: Impedance to displacement of transducer base, Z_r, when: —— open-circuit; – – – $R_e + R_s = 0$, $L_e + L_s = -1$ mH; – - – - $R_e + R_s = -0.7\ \Omega$, $L_e + L_s = -1$ mH; —□— $R_e + R_s = 0$, $L_e + L_s = 1$ mH; · · · · · · $R_e + R_s = -0.7\ \Omega$, $L_e + L_s = 1$ mH.

2.2. Instability

As demonstrated above, in order to tune the resonance of the shunted transducer down in frequency, the total circuit inductance must be negative. A shunted transducer with a total circuit impedance with positive real and negative parts is inherently stable, however, with a total circuit impedance that has negative real or imaginary parts the shunt could introduce instability if not properly designed. This is because a complex impedance with negative real or imaginary components requires energy input to the system to reverse the direction of current flow and, therefore, is an active component. The stability of the system can be evaluated by considering the poles of the shunted transducer's response. The Laplace domain transfer function, $H(s)$, of the SDOF shunted transducer model shown in Figure 2, with a harmonic force acting on the mass, can be expressed as

$$H(s) = \frac{1}{m_r s^2 + b_r s + k_r + \frac{s(Bl)^2}{(R_e+R_s)+s(L_e+L_s)}}, \tag{2}$$

where s is the complex frequency. This system will be unstable when any of the system poles have a positive real part. It can be demonstrated by equating the denominator of equation 2 to zero and rearranging, that if the total circuit resistance, R_{total}, where $R_{total} = R_e + R_s$, has a different sign to the total circuit inductance, L_{total}, where $L_{total} = L_e + L_s$, then there will always be a positive real root and the system will be unstable. Conversely, it is important to note that the system is always stable when R_{total} and L_{total} are both positive. However, when R_{total} and L_{total} are both negative, a complex problem is formed and the stability of the system is dependent on the system parameters and can only be determined by calculating the system poles.

Based on this analysis of the system poles, instabilities can be avoided during the design process. However, if this is carried out based on purely nominal transducer parameter values, then the system may become unstable in the presence of uncertainty. Therefore, in order to design a system that is robustly stable, uncertainties must be taken into account when designing the shunt circuit if R_{total} and L_{total} are negative.

3. Characterisation of the variation in miniature electrodynamic transducers

As stated in the introduction, this study examines a novel design process, where realistic uncertainties in the transducers are considered directly during the optimisation procedure, with the aim of achieving a level of robustness to these uncertainties. Therefore, a knowledge of the realistic uncertainties present in these transducers, and their effect on the shunted response and the robustness, is first required. Tolerances are given for the parameters in the manufacturer's data sheet [17], however, the distribution of values within these tolerances is not provided. In order to include a realistic representation of the variation in the transducers used, the parametric variation is characterised experimentally. In this section, the procedure and results of the experimental characterisation are set out, before the effect of the shunt impedance on the mechanical response of an electrodynamic inertial transducer is described.

A total of 59 transducers were obtained and their dynamic and electrical responses were measured in order to estimate the variation in their effective parameters. The parameters identified, which are required for the analytical representation set out in Figure 2, are: resonance frequency, f_r; moving mass, m_r; suspension stiffness, k_r; damping ratio, ζ (the damping coefficient b_r can be calculated from this as $b_r = 2\zeta\sqrt{k_r m_r}$); transduction coefficient, Bl; coil resistance, R_e; and coil inductance, L_e. The methods for measuring and calculating each of the parameters are set out in the Appendix Appendix A.

The results of the experimental characterisation of the transducer parameters are summarised in Figure 5, which shows plots of the distributions of each of the identified parameters. From these results it can be seen that each of the parameters can be approximated by a normal distribution curve. It should be noted that the distribution of the identified stiffness, k_r, is not shown in Figure 5 because it is simply related to the mass, m_r, and resonance frequency, f_r. In the following section, the effect of these measured variations in the transducer parameters on their shunted response will be presented.

3.1. The effect of the characterised transducer uncertainty on the tuned transducer response

In order to investigate the effect of the characterised transducer variations on their shunted responses, the free-vibration response of the shunted transducer shown in Figure 2 can be expressed as

$$m_r \ddot{w}_r(t) = k_r w_r(t) + \left(b_r + \frac{(Bl)^2}{(R_e + R_s + j\omega(L_e + L_s))} \right) \dot{w}_r(t), \tag{3}$$

where $w_r(t)$ is the displacement of the transducer mass. An initial investigation into the effect of the transducer parameter variations highlighted that the shunted transducer response was most sensitive to variations in the DC resistance of the coil, R_e, and the transduction coefficient, Bl, and therefore,

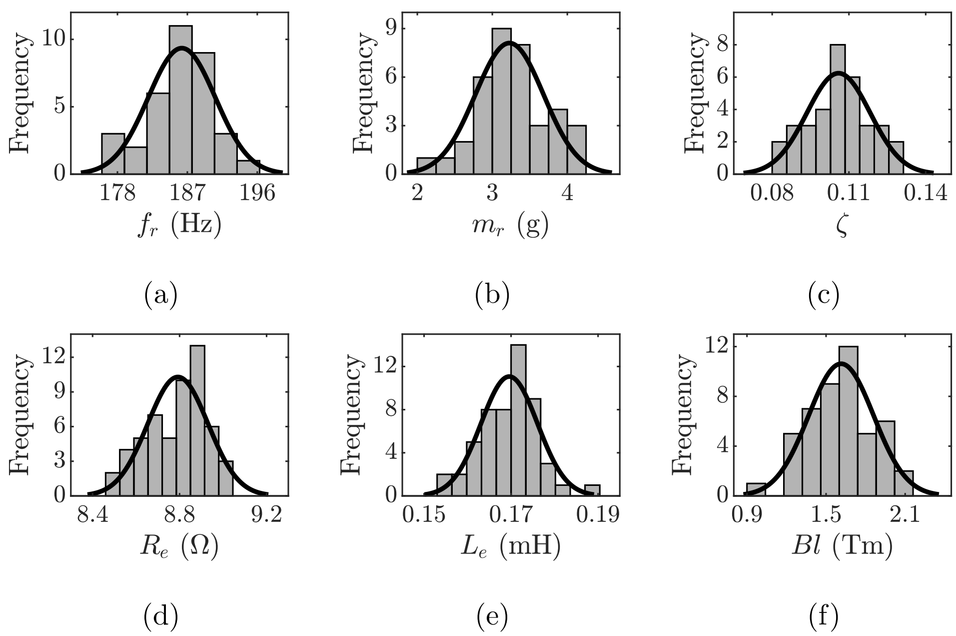

Figure 5: Histograms with approximated normal distribution curve for the identified transducer properties: (a) f_r, (b) m_r, (c) ζ, (d) R_e, (e) L_e, (f) Bl.

for conciseness, the following results focus on these two parameters. Figures 6 and 7 show the effect of variation in R_e and Bl respectively, for two different shunted resonance frequencies, 175 Hz in plot (a) and 150 Hz in plot (b) in both figures. In each case, variations of ± 1 and ± 2 standard deviations of the measured distributions, σ, are shown and the results focus on the effect of tuning the resonance frequency down from the open circuit resonance of 187 Hz since the effect is simply mirrored for an increase in the resonance frequency. In Figures 6.a and 7.a, where the resonance frequency has only been tuned down by around 6.5%, it can be seen that for all variations shown there is little to no change in the response. However, when the transducer is tuned down by approximately 20%, to 150 Hz, the variations in the response are much greater. For uncertainty in the coil resistance, R_e, Figure 6.b shows a small change in the frequency of the peak, and a significant change in the damping. Similarly, for uncertainty in the transduction coefficient, Bl, Figure 7.b shows increased damping and a shift in the resonance frequency, which is correlated to the magnitude of the change in Bl. From these results, it can be concluded that the effect of the transducer parameter variation is greater the further the shunted resonance is from the open-circuit resonance frequency.

The results presented in Figures 6-7 suggest that uncertainty in R_e and Bl will limit the accuracy of the tuned response. To improve the accuracy of the tuned response, it would be necessary to reduce the acceptable manufacturing tolerances on the resistance of the coil or transduction coefficient. In terms of the voice coil resistnace, R_e, however, the measured variation was within approximately $\pm 5\%$ of the mean, which is in line with what is expected for machine wound voice coils [19] and, therefore, reducing the variation is likely to significantly increase production costs.

Considering the variation in the transduction coefficient, Bl, it is clear from the measurement results presented in Figure 5.f and the resulting variation in the shunted resonator impedances presented in Figure 7, that the wide range of variation in Bl ($\approx \pm 40\%$) results in significant variation in the tuned response. The large range of variation in Bl could be due to the fact that several measurements are required to estimate this parameter, which may multiply the effect of any inaccuracies due to noise or imperfect measurement conditions (for example, out-of-plane motion). It could also be a result of the low-cost manufacturing used for the considered transducers, which could result in inconsistencies in the relative position of the magnet with respect to the coil. In motion, the position of the coil within the magnetic field also changes, which means that Bl is actually dependent on displacement. This dependency and its effect on the shunt impedance are not the focus of this work and instead a tuning method will be developed to provide robustness to the uncertainty in Bl, and this is described in Section 5.

4. Dynamics of a Vibrating Structure with an attached EDMM

In order to investigate the performance of the EDMM proposed in Section 2 for the control of structural vibration, this section will introduce a model of a structure. For the specific example considered here of a unit cell of 12 resonators, as shown in Figure 1, we aim to control 3 adjacent modes of an attached structure, and, therefore, define a 3DOF system. The concept and design process, however, can be straightforwardly extended to higher order systems. The 3DOF structure consists of three equally distributed masses suspended in series between fixed boundaries by four equal translational spring elements with a structural (hysteretic) loss factor, as shown in Figure 8. A unit cell of the EDMM is attached to each mass element, oriented such that the masses of the EDMM move along the same axis as the masses of the structure, as also shown in Figure 8. In this section, the analytical model used to simulate the dynamics of the system, and to evaluate the EDMM optimisation procedure, is first set out. The response of the structure without the EDMM is then evaluated, and the introduction of structural uncertainties is explained and defined.

4.1. Formulation

The response of the 3DOF structure, shown in Figure 8, without the EDMM attached can be expressed as

$$\mathbf{F}(t) = (1 + \mathrm{j}\eta)\mathbf{K}\boldsymbol{w}(t) + \mathbf{M}\ddot{\boldsymbol{w}}(t), \tag{4}$$

where η is the hysteretic damping loss factor,

$$\mathbf{F}(t) = \begin{bmatrix} 0 \\ 0 \\ F(t) \end{bmatrix}, \mathbf{K} = \begin{bmatrix} 2k & -k & 0 \\ -k & 2k & -k \\ 0 & -k & 2k \end{bmatrix}, \mathbf{M} = \begin{bmatrix} m & 0 & 0 \\ 0 & m & 0 \\ 0 & 0 & m \end{bmatrix},$$

$$\text{and } \boldsymbol{w}(t) = \begin{bmatrix} w_1(t) \\ w_2(t) \\ w_3(t) \end{bmatrix}.$$

$w_n(t)$ is the displacement of the n-th mass. The action of the EDMM can then be expressed as an additional opposing force vector, $\mathbf{F}_{\boldsymbol{r}}(t)$, where

$$\mathbf{F}_{\boldsymbol{R}}(t) = \begin{bmatrix} F_{R,\,1}(t) \\ F_{R,\,2}(t) \\ F_{R,\,3}(t) \end{bmatrix} = Z_R\boldsymbol{w}(t).$$

$F_{R,\,n}(t)$ is the total force due to the n-th EDMM acting on the n-th mass respectively, and Z_R is the total impedance of the base of the EDMM to a displacement. The equation of motion for the structure with the EDMM attached can therefore be expressed as

$$\mathbf{F}(t) - \mathbf{F}_{\boldsymbol{R}}(t) = (1 + \mathrm{j}\eta)\mathbf{K}\boldsymbol{w}(t) + \mathbf{M}\ddot{\boldsymbol{w}}(t). \tag{5}$$

As the EDMM unit cell consists of 12 shunted transducers with the same base reference, the EDMM force acting on the n-th mass, $F_{R,\,n}(t)$, due to $w_n(t)$, can be expressed as the sum of the forces and impedances due to each individual transducer, $F_r(t)$ and $z_r(t)$ respectively, as

$$F_{R,\,n}(t) = Z_R w_n(t) = \sum_{r=1}^{12} F_{r,\,n}(t) = \sum_{r=1}^{12} Z_r w_n(t). \tag{6}$$

If it is assumed that the individual shunted transducers that form the EDMM can be approximated by the model shown in Figure 2, then $F_{r,\,n}(t)$ can be expressed as

$$\begin{aligned} F_{r,\,n}(t) &= k_r\Big(w_n(t) - w_r(t)\Big) + \left(b_r + \frac{(Bl)^2}{Z_{es}}\right)\Big(\dot{w}_n(t) - \dot{w}_r(t)\Big) \\ &= Z_r w_n(t), \end{aligned} \tag{7}$$

where $w_r(t)$ is the displacement of the transducer mass, and Z_{es} is the total electrical impedance of the shunted voice coil ($Z_{es} = (R_e+R_s)+\mathrm{j}\omega(L_e+L_s)$). The response of the system at each frequency can be evaluated by assuming a linear system undergoing time-harmonic motion, where $F_{r,\,n}(t)$, $w_n(t)$ and $w_r(t)$ are equal to $\tilde{F}_{r,\,n}e^{\mathrm{j}\omega t}$, $W_n e^{\mathrm{j}\omega t}$ and $W_r e^{\mathrm{j}\omega t}$ respectively, where $\tilde{F}_{r,\,n}$, W_n and W_r are complex amplitudes, then equation 7 can be expressed as

$$\tilde{F}_{r,\,n} = \left(k_r + \mathrm{j}\omega b_r + \mathrm{j}\omega\frac{(Bl)^2}{Z_{es}}\right)(W_n - W_r) = Z_r W_n. \tag{8}$$

W_r can be evaluated by considering the equation of motion of the transducer in Figure 2, which when subject to base excitation in the form of $w_n(t)$ can be expressed as

$$m_r \ddot{w}_r(t) = k_r\Big(w_n(t) - w_r(t)\Big) + \left(b_r + \frac{(Bl)^2}{Z_{es}}\right)\Big(\dot{w}_n(t) - \dot{w}_r(t)\Big), \tag{9}$$

which, when $w_n(t) = W_n e^{\mathrm{j}\omega t}$ and $w_r(t) = W_r e^{\mathrm{j}\omega t}$, becomes

$$-\omega^2 m_r W_r = \left(k_r + \mathrm{j}\omega b_r + \frac{(Bl)^2}{Z_{es}}\right)(W_n - W_r). \tag{10}$$

Equation 10 can be rearranged to give an expression for W_r in terms of the transducer dynamics and the base displacement as

$$W_r = \frac{k_r + \mathrm{j}\omega b_r + \mathrm{j}\omega \frac{(Bl)^2}{Z_{es}}}{k_r + \mathrm{j}\omega b_r + \mathrm{j}\omega \frac{(Bl)^2}{Z_{es}} - \omega^2 m_r} W_n. \tag{11}$$

Substituting equation 11 into equation 8 gives

$$\tilde{F}_{r,\,n} = Z_{sr}\left(1 - \frac{Z_{sr}}{Z_{sr} + \omega^2 m_r}\right) W_n, \tag{12}$$

where

$$Z_{sr} = k_r + \mathrm{j}\omega b_r + \mathrm{j}\omega \frac{(Bl)^2}{Z_{es}}, \tag{13}$$

and this therefore leads to an expression for Z_r as

$$Z_r = Z_{sr}\left(1 - \frac{Z_{sr}}{Z_{sr} + \omega^2 m_r}\right). \tag{14}$$

Combining Equations 5, 6 and 14 gives

$$\mathbf{F}(t) = \left((1 + \mathrm{j}\eta)\mathbf{K} + \sum_{r=1}^{12} Z_r \boldsymbol{I}\right)\boldsymbol{w}(t) + \mathbf{M}\ddot{\boldsymbol{w}}(t), \tag{15}$$

where $\boldsymbol{I}$ is a 3×3 identity matrix. Assuming the driving force is harmonic ($\mathbf{F}(t) = \tilde{\mathbf{F}}e^{\mathrm{j}\omega t}$) then the vector of structural velocity amplitudes at frequency ω can be expressed as

$$\dot{\boldsymbol{W}}(\omega) = \left(\frac{1}{\mathrm{j}\omega}\left((1+\mathrm{j}\eta)\mathbf{K} + \sum_{r=1}^{12} Z_r(\omega)\boldsymbol{I}\right) + \mathrm{j}\omega\mathbf{M}\right)^{-1}\tilde{\mathbf{F}}(\omega) \qquad (16)$$

The total kinetic energy of the structure, $E_k(\omega)$ can then be calculated by

$$E_k(\omega) = \frac{1}{2}\omega\dot{\boldsymbol{W}}^{\mathrm{H}}(\omega)\mathbf{M}\dot{\boldsymbol{W}}(\omega), \qquad (17)$$

where superscript H indicates the Hermitian transpose. The total attenuation in structural kinetic energy over frequency achieved by the EDMM can therefore be expressed, in decibels, as

$$E_{k,\,atten} = 10\log_{10}\left(\sum^{\omega}\frac{\dot{\boldsymbol{W}}^{\mathrm{H}}(\omega)\dot{\boldsymbol{W}}(\omega)}{\dot{\boldsymbol{W}}_{\mathbf{0}}{}^{\mathrm{H}}(\omega)\dot{\boldsymbol{W}}_{\mathbf{0}}(\omega)}\right), \qquad (18)$$

where $\dot{\boldsymbol{W}}_{\mathbf{0}}$ is the vector of structural velocities without the EDMM attached, where $\sum_{r=1}^{12} Z_r(\omega) = 0$.

4.2. Defining the structure and its uncertainties

As discussed in Section 3.1, the effect of the uncertainties in the electrical characteristics of the transducer is greater the larger the difference between the shunted resonance frequency and the open-circuit resonance frequency. Therefore, in practice, the transducer should be selected to suit the scale and the frequency response of the structure. For example, a heavy structure with problematic low frequency resonances will require transducers capable of a greater force and with a lower resonance frequency than a lightweight structure with higher frequency resonances. Therefore, in order to evaluate the performance of the proposed EDMM using the transducers considered in Section 3, the 3DOF structure to be controlled is designed so that its structural modes are set within a bandwidth covering the open-circuit resonance of the transducer. Based on the robustness to variation in R_e alone, this bandwidth is set so that the structural modes fall within $\pm 20\%$ of the nominal shunted resonance, which corresponds to a bandwidth of 100 – 460 Hz. The mass of the 3DOF structure is set so that the added mass due to all three EDMM unit cells equates to approximately 10% of the total structural mass and a 1% structural damping ratio, corresponding to $\eta = 0.02$, is used.

In addition to variations in the transducer parameters, it is practically relevant to consider the effect of potential variations in the structure itself. The manifestation of uncertainties in a practical structure would be dependent on the size, construction methods, manufacturing tolerances, use, amongst many other variables. Therefore, it is not straightforward to define uncertainties for a general case study. However, in a structure such as a beam or a plate, the dimensions of the structure affect both its mass and stiffness. To this end, a normalised 'effective thickness', h_{eff}, is introduced, which is equal to 1 in the nominal case. A $\pm 10\%$ bounded, uniformly-distributed uncertainty in the normalised effective thickness, h_{eff}, is considered. This is not representative of any uncertain structure in particular, but it is a generic parametric uncertainty that will be representative of the effect of realistic uncertainty, in that the total mass of the structure and the natural frequencies will be modified. The mass of a simple beam or plate is proportional to its thickness, and the one-dimensional flexural stiffness is proportional to the thickness cubed. Therefore, the mass of each element is multiplied by

h_{eff} and the translational stiffnesses are multiplied h_{eff}^3 in order to achieve each uncertain case. Figure 9 shows the total kinetic energy of the nominal structure, E_k, in black, and the variation in the kinetic energy due to the defined structural uncertainty in grey. It can be seen from these results how the resonance frequencies shift in the presence of structural uncertainties.

5. Optimisation of the Robust EDMM Performance

Optimising the shunt impedance of multiple shunted transducers in order to achieve a high level of performance in the presence of parametric uncertainty in both the structure to be treated and the transducers themselves presents a highly complex, multi-variable design problem. A manual or iterative approach to the design would be time-consuming and labour intensive. Instead, metaheuristic optimisation algorithms, such as evolutionary or swarm algorithms, could be used to optimise the various design parameters [20]. Metaheuristics combine a low-level problem, i.e. changing a parameter to find the minimum of a solution, with higher-level functions, such as combining multiple sets of variables or stochastic variation. These methods have the benefit of requiring very little initial information and can find high-achieving solutions to a complex multi-dimensional in a fraction of the time compared to an exhaustive search. Metaheuristics have been used in the topological design of single resonator metamaterials [21, 22, 23], but this is computationally demanding, requiring complex finite element models to be run for each iteration, and this complexity would be further increased in the case of a multi-resonator unit cell. However, in the case of the EDMM considered here, the shunted resonator design can be modelled analytically to a reasonable degree of accuracy and thus a metaheuristic approach is well suited to directly optimise the shunt parameters to maximise performance.

This section sets out the optimisation procedure utilised here and the results of the optimisation study. Firstly, the optimisation problem is described, along with a justification for the chosen optimisation algorithm. The successive subsections then go on to describe the implementation of the algorithm, set out the optimisation procedure and configuration in more detail, and then present the results for discussion.

The EDMM needs to be tuned as a whole, with a single total impedance frequency response function. This is achieved by setting the shunt circuit parameters for each of the 12 transducers in the unit cell, which corresponds to a total of 24 variables corresponding to the resistance, R_s, and inductance, L_s, of the shunt impedance for each transducer. Designing this response for robust performance adds a further level of complexity to the optimisation problem, since the performance must be considered under a range of conditions. This problem is well suited to a metaheuristic approach, as no prior knowledge of how to set the variables is required, and the combination of stochastic processes and intelligent search mechanisms can produce high-performing results in a fraction of the time of an exhaustive search [20]. In this study a particle swarm optimisation (PSO) is used to find high-performing configurations. This has been shown in similar studies by the authors to perform well, both in terms of the output, but also in terms of the computation time [24]. The PSO is often also favoured for its relative simplicity when compared to other optimisation approaches such as the genetic algorithm [25].

5.1. Constrained Particle Swarm Optimisation (PSO)

The PSO is implemented using a constrained particle swarm implementation in MATLAB [26], which uses an algorithm based on the original Kennedy and Eberhart design [27] and constraints are added using a penalty function [28]. A population of N particles is optimised, and on each iteration, the particle 'positions' are updated based on the current velocity vectors. The fitness values are then calculated for each of the new positions, and two types of constraint, bounds and non-linear inequality constraints, are imposed using a penalty function. The penalised fitness vector for the n-th individual in the current population, $J_{pen,\,n}$, can be expressed as

$$J_{pen,\,n} = J_n + \sum \left(\frac{\bar{\boldsymbol{J}} \boldsymbol{g}_n^{\mathrm{T}} \boldsymbol{g}_n}{\sum^{N} \bar{\boldsymbol{g}}_n^2} \right) + J_{worst,\,feasible}, \tag{19}$$

where J_n is the unpenalised fitness value, $\bar{\boldsymbol{J}}$ is the mean of the unpenalised fitness values of the new population, $\boldsymbol{g}_n$ is the vector of constraint values that have not been met for the n-th individual, $\bar{\boldsymbol{g}}_n$ is the mean value of the vector $\boldsymbol{g}_n$, and $J_{worst,\,feasible}$ is the worst fitness value from all feasible members (those which meet all constraints) of the new population. This final term ensures that feasible positions will always have a smaller fitness value than unfeasible positions. Following this, the velocity of each particle is updated based on a weighted combination of the particle's current velocity, and the distances to the best scoring position within a randomly selected sub-population, and the best historical position of the particle. Further details on the constrained PSO can be found at [26].

5.2. Optimisation Procedure

The aim of the optimisation is to minimise the output of a fitness function. For this study, the aim is to maximise the broadband attenuation in the structural response provided by the EDMM to an unknown disturbance, and therefore the fitness function, J, is defined as the inverse of the mean total attenuation in kinetic energy, $\overline{E}_{k,\,atten}$, calculated using Equation 18 over M uncertain structure-transducer models. This can be expressed as

$$J = -\overline{E}_{k,\,atten} = -\frac{1}{M}\sum_{m=1}^{M} E_{k,\,atten,\,m}, \tag{20}$$

where $E_{k,\,atten,\,m}$ is the total attenuation in kinetic energy of the m-th uncertain structure-transducer models, calculated using the formulation set out in Section 3; by minimising the inverse of $\overline{E}_{k,\,atten}$, the mean total attenuation is maximised. Although this approach only considers the frequency domain response, because the system is linear, the frequency domain response is representative of the dynamic response to any disturbance in the time domain.

The EDMM is first optimised for the nominal responses only to give a benchmark against which to compare the robust performance of the robustly optimised EDMMs. Three strategies for robustly optimising the EDMMs are considered as follows: optimisation with uncertainties in the structure alone; optimisation with uncertainties in the transducers alone; and optimisation considering uncertainties in both the structure and the transducers. The robust performance of each optimised configuration is then evaluated for the case where there are uncertainties in both the structure and the transducers, giving insight into the importance of considering each type of uncertainty.

For the robust optimisations, a total of 120 cases are considered. These

120 cases comprise of the nominal case with no uncertainty in the structure or transducers, plus 119 additional cases with uncertainties introduced. For the optimisation where only uncertainties in the structure are considered, the transducer parameters in each case are set to their nominal values, and for the optimisation where only uncertainties in the transducers are considered, the structure in each case is specified according to the nominal parameters. The structural uncertainties are defined by equidistant points along the defined normalised effective thickness distribution, as described in Section 4.2. The parameters of each individual transducer in the uncertain cases are selected at random from the distributions set out in Section 4, and bounded to $\pm 2\sigma$ as the distribution alone can produce values outside of the measured range. This randomised uncertainty is reproduced and therefore consistent on every run of the optimisation, this ensures that any differences between configurations cannot be attributed to differences in the allocation of the starting population.

The shunt impedance corresponding to each shunted transducer is optimised consecutively, and additively. This approach achieved a marginally better result than optimising all transducers simultaneously, without a significant increase in computation time as the number of generations required to find a solution significantly decreases.

The optimisation constraints are set at follows. Firstly, it should be possible for the transducers to be tuned anywhere within the 100-460 Hz range that contains the dominant features of the considered structural response, as shown in Figure 9, and the shunted transducers should allow a range of damping values. In order to achieve this, the shunt resistance, R_s, and inductance,

L_s, values are bounded within $-12 \leq R_s \leq -4\ \Omega$ and $-10 \leq L_s \leq 10$ mH respectively. Secondly, the total resistance and total inductance must also be constrained to ensure stability, as discussed in Section 2.2. Specifically, the system will always be unstable if the total resistance and total inductance have opposite signs, and, therefore, a constraint is imposed that requires the negative ratio of the shunt resistance to the shunt inductance, $-R_s/L_s$, to be less than zero. Instability may also occur when the total resistance and total inductance are both negative, but in this case stability must be ensured by constraining the real parts of the poles in the transfer function of the shunted transducer to be less than zero for all transducer uncertainties.

In addition to the fitness function and constraints, there are a number of other PSO algorithm settings, which can be used to modify the behaviour of the optimisation. Firstly, in this study, the velocity update function is weighted towards the local and historical best positions over the current position by a factor of two. This promotes exploration by enabling faster movement across the solution space even in the presence of similar fitness. The initial inertias are also configured with a large upper limit to enhance exploration early on in the optimisation run. A swarm size of 300 is used, and the optimisation runs until the best fitness does not improve by more than 0.01 dB over the previous 30 iterations, thus ensuring that the optimisation reaches a good solution. Initial investigations were used to confirm that the algorithm generates consistent final fitness values when it was run from different sets of start points, so that a single set of start points could be used to evaluate the performance of the different approaches. This initial investigation confirmed that the fitness value achieved from different starting points were within 0.1 dB of each other.

5.3. Optimisation Results and Discussion

In the preceeding sections, an optimisation procedure has been set out for the design of an EDMM that is robust to parametric uncertainties. This section presents and analyses the results of this approach, and compares them to the results for the EDMM optimised for nominal performance alone, the EDMM left open-circuit, and the case when an inert mass of equal magnitude to the EDMM is added to the structure. The mean attenuation over the 120 uncertain structure-transducer cases, $\overline{E}_{k,\,atten}$, for each approach is presented in Figure 10, along with the standard deviation in the case-by-case performance, $\sigma(E_{k,\,atten})$. It can be seen from these results that the configurations optimised for all uncertainties and for transducer uncertainties only achieve the greatest $\overline{E}_{k,\,atten}$, and also show the least variation between cases, as dictated by the low $\sigma(E_{k,\,atten})$; the only exception to this observation being the low standard deviation achieved with the added mass configuration, but the level of attenuation in this case is very limited. The configurations optimised for nominal performance and structural uncertainties alone achieve poor robustness when both structural and transducer uncertainties are included, and perform notably worse in comparison to the open-circuit EDMM in both $\overline{E}_{k,\,atten}$ and $\sigma(E_{k,\,atten})$.

To provide more insight into the performance achieved by the different conditions presented in Figure 10, Figure 11 shows the performance of each optimisation procedure over all 120 uncertain structure-transducer cases (——), sorted by the normalised effective thickness parameter used to characterise the structural uncertainty: Figure 11.a shows the performance of the configuration optimised for nominal performance; Figure 11.b shows the performance of the configuration optimised for robustness to structural uncertainties; Figure 11.c shows the performance of the configuration optimised for robustness to transducer uncertainties; Figure 11.d shows the performance of the configuration optimised for robustness to all uncertainties. Each case is also compared to the performance of the EDMM when it is left un-shunted, in the open-circuit state (dashed), and when the EDMM is replaced with an equivalent additional mass only (dotted). The data presented in Figure 11 also shows any individual cases where one or more instabilities are present in the EDMM - these cases are highlighted with a red dot. It can be seen from the results presented in Figures 11.a and 11.b respectively, that optimising the design for either the nominal response or when only considering the structural uncertainties, fails to achieve robustness in the presence of uncertainties in the transducers, with significant enhancements in kinetic energy ($E_{k,\,atten} < 0$), accounting for the low $\sigma(E_{k,\,atten})$ seen in Figure 10. Additionally, for these two configurations, there are also instabilities in all cases other than the nominal system, which means that there is a danger of not only amplifying the structural response, but of damaging the transducers or the circuitry. In comparison, the results presented in 11.c for the configuration optimised considering only the transducer uncertainty demonstrate robustness to structural uncertainty, and instabilities are completely avoided. Finally, when all uncertainties are taken into account during the optimisation, as shown by the results presented in 11.d, the robust performance is almost identical to the optimisation only considering transducer uncertainty. These results suggest that the robustness is dominated by the uncertainty in the transducers, and that structural uncertainty could be neglected in this case. To further investigate why this apparent difference in sensitivities is present, the impedance of the optimised EDMM as presented to the structure, Z_R, is examined.

Figure 12 shows Z_R over frequency for the nominal transducer (black-solid) and the transducers with uncertainty (dashed, grey if stable, red if unstable) when optimised for (a) structural uncertainty only, (b) transducer uncertainty only, and (c) both structural and transducer uncertainties. As expected, it can be seen that there is significantly more variation in Z_R due to transducer uncertainty when this is not considered directly in the optimisation. For the optimisation configurations that consider either transducer uncertainty alone or both structural and transducer uncertainties have resulted in very similar results, with no visible resonance other than a small hump around the open-circuit resonance. This suggests that rather than significantly shifting the resonance frequency, the shunts have been used to obtain damped responses from the 12 unit cell transducers. The resulting highly damped response explains why the structural uncertainties have very little effect on the robustness of these two optimised configurations, as the performance of the EDMM is almost independent of frequency, with only a slight tail-off at lower frequencies. It is worth noting that if these instabilities result in permanent transducer failure, then they are not viable solutions, and therefore for an optimisation approach to be viable the transducer uncertainties must be taken into account.

6. Conclusions

In this work, a shunted electrodynamic metamaterial (EDMM) vibration absorber has been proposed, with a unit cell consisting of an array of 12 shunted inertial electrodynamic transducers. In order to assess the practicability of the proposed system, the variations in a low-cost, commercially available inertial transducer were characterised experimentally, and this information was used to evaluate the robustness of the shunting to these uncertainties both in terms of the resulting change in the frequency response and also in terms of stability. An analysis of the response of the shunted inertial transducers has shown that it becomes unstable under certain conditions and that this must therefore be considered in the design approach, particularly in the presence of transducer uncertainties. Finally, a method of optimising the tuning of the EDMM for robustness to uncertainties in both the structure to be controlled, and the transducers has been proposed. The resulting performance of the optimised EDMM under different conditions has demonstrated that it is essential to include the transducer uncertainties in the optimisation procedure, because otherwise the system becomes unstable when practical transducer uncertainties occur. However, the structural uncertainties considered in this study can be neglected during the optimisation, since optimising for robust performance based on transducer uncertainties alone ensures robustness to the considered structural uncertainties because of the resulting highly damped EDMM. The EDMM optimised taking into account uncertainties was shown to achieve a higher level of robust performance compared to an EDMM optimised without any uncertainties considered, and compared to the open-circuit EDMM.

Acknowledgments

This research was partially supported by an EPRSC iCASE studentship (Voucher number 17100092) and the Intelligent Structures for Low Noise Environments (ISLNE) EPSRC Prosperity Partnership (EP/S03661X/1).

The authors acknowledge the use of the IRIDIS High Performance Computing Facility, and associated support services at the University of Southampton, in the completion of this work.

Appendix A. Methods for the experimental characterisation of the inertial transducers

In order to characterise the inertial transducers used, two experiments were carried out:

Experiment 1 - In order to measure the response to dynamic excitation, the transducers are clamped in turn to the platform of a large shaker, as shown in Figure A.13.(a, c, d). The shaker is driven with white noise and the acceleration of the base platform, $\ddot{w}_0(t)$, is measured with an accelerometer. Simultaneously, a laser vibrometer is used to measure the velocity of the magnet mass of the transducer, $\dot{w}_r(t)$.

Experiment 2 - A second experimental configuration is used to measure the response of the transducers to electrical excitation. The individual transducers are each connected in series with a resistance, R, of 10 Ω, as shown in Figure A.13.(b), and the circuit is driven with white noise. The total voltage across the circuit, $v_{total}(t)$, and the voltage across the resistor, $v_R(t)$, are both measured.

Appendix A.1. Estimation of the moving mass and dynamic stiffness

The response of the shaker and transducer are captured without modification, and also with a 200 μg mass added to the top of the transducer magnet to introduce a shift in the resonance frequency. The peak in the frequency domain transfer response magnitude between the base acceleration and mass velocity is taken as the resonance frequency in each case and the change in resonance frequency due to the additional mass can be used to calculate the mass and stiffness of the transducers as follows.

The open-circuit resonance frequency in Hertz, f_r, of an ideal SDOF inertial transducer can be approximated as

$$fr = \frac{1}{2\pi}\sqrt{\frac{k_r}{m_r}}, \tag{A.1}$$

where k_r is the stiffness of the suspension and m_r is the moving mass. Increasing the moving mass with the addition of m_{load}, therefore lowers the resonance frequency to a new value, f_m, and equation A.1 becomes

$$f_m = \frac{1}{2\pi}\sqrt{\frac{k_r}{m_r + m_{load}}}. \tag{A.2}$$

These simultaneous equations can be solved for k_r and m_r.

Appendix A.2. Estimation of the damping coefficient

The damping ratio ζ_r can be estimated using the half-power method [29], defined as

$$\zeta_r = \frac{\omega_2 - \omega_1}{2\omega_r} = \frac{f_2 - f_1}{2f_r}, \tag{A.3}$$

where f_1 and f_2 refer to the frequencies above and below resonance respectively, where the power is half of that at resonance.

Appendix A.3. Estimation of the electrical impedance of the coil

With the mass of the transducers prevented from moving, assuming that the measured voltages as shown in Figure A.13.b are harmonic, so that $v_{total}(t) = V_{total}e^{j\omega t}$ and $v_R(t) = V_R e^{j\omega t}$, then the blocked electrical impedance, $Z_{eb}(j\omega)$, can be calculated as

$$Z_{eb}(j\omega) = R\left(\frac{V_{total}}{V_R} - 1\right). \tag{A.4}$$

It is assumed that the coil can be modelled as a resistor, R_e, and inductor, L_e, connected in series with $Z_{eb}(j\omega) = R_e = j\omega L_e$. Thus at low frequencies, where $R_e >> \omega L_e$, $Z_{eb} \approx R_e$. At high frequencies L_e can then be estimated for a given frequency as $L_e = \sqrt{\frac{|Z_{eb}(j\omega)|^2 - R_e^2}{\omega^2}}$.

Appendix A.4. Estimation of the transduction coefficient

The transduction coefficient, or force factor, Bl, can be estimated using the procedure described in [30], where assuming the effect of eddy currents is negligible, it can be expressed as

$$Bl = \left(\mathbb{R}\left\{Z_e(j\omega_r)\right\} - R_e\right)\frac{I(j\omega_r)}{\dot{W}_r(j\omega_r)} \tag{A.5}$$

where $Z_e(j\omega_r)$ is the free-mass electrical impedance of the transducer, $I(j\omega_r)$ is the current through the coil and $\dot{W}_r(j\omega_r)$ is the velocity amplitude of the moving mass, all measured at the resonance frequency ω_r. In reality Bl will be dependent on the position of the coil within the magnetic field and the presence of eddy currents, so the value calculated by this approach is only a linear approximation.

References

[1] J. Ormondroyd, J. P. Den Hartog, The Theory of the Dynamic Vibration Absorber, Journal of Applied Mechanics 50 (1928) 9–22.

[2] T. Igusa, K. Xu, Vibration Control Using Multiple Tuned Mass Dampers, Journal of Sound and Vibration 175 (4) (1994) 491–503. doi:10.1006/JSVI.1994.1341.
URL https://www.sciencedirect.com/science/article/pii/S0022460X84713411

[3] S. Dalela, P. S. Balaji, D. P. Jena, A review on application of mechanical metamaterials for vibration control, Mechanics of Advanced Materials and Structures (2021) 1–26doi:10.1080/15376494.2021.1892244.
URL https://www.tandfonline.com/action/journalInformation?journalCode=umcm20

[4] H. Sun, X. Du, P. F. Pai, Theory of Metamaterial Beams for Broadband Vibration Absorption, Journal of Intelligent Material Systems and Structures 21 (11) (2010) 1085–1101. doi:10.1177/1045389X10375637.
URL http://journals.sagepub.com/doi/10.1177/1045389X10375637

[5] Y. Xiao, J. Wen, X. Wen, Broadband locally resonant beams containing multiple periodic arrays of attached resonators, Physics Letters A 376 (16) (2012) 1384–1390. doi:10.1016/J.PHYSLETA.2012.02.059.
URL https://www.sciencedirect.com/science/article/pii/S037596011200254X

[6] R. Zhu, X. Liu, G. Hu, C. Sun, G. Huang, A chiral elastic metamaterial beam for broadband vibration suppression, Journal of Sound and Vibration 333 (10) (2014) 2759–2773. doi:10.1016/J.JSV.2014.01.009.
URL `https://www.sciencedirect.com/science/article/pii/S0022460X14000315#bib14`

[7] H. Peng, P. Frank Pai, H. Deng, Acoustic multi-stopband metamaterial plates design for broadband elastic wave absorption and vibration suppression, International Journal of Mechanical Sciences 103 (2015) 104–114. doi:10.1016/J.IJMECSCI.2015.08.024.
URL `https://www.sciencedirect.com/science/article/pii/S0020740315003136`

[8] G. W. Milton, J. R. Willis, On modifications of Newton's second law and linear continuum elastodynamics, Proceedings of the Royal Society A: Mathematical, Physical and Engineering Sciences 463 (2079) (2007) 855–880. doi:10.1098/rspa.2006.1795.
URL `https://royalsocietypublishing.org/doi/10.1098/rspa.2006.1795`

[9] S. Yao, X. Zhou, G. Hu, Experimental study on negative effective mass in a 1D mass–spring system, New Journal of Physics 10 (4) (2008) 043020. doi:10.1088/1367-2630/10/4/043020.
URL `http://stacks.iop.org/1367-2630/10/i=4/a=043020?key=crossref.c927b94d8f96`

[10] P. F. Pai, Metamaterial-based Broadband Elastic Wave Absorber, Journal of Intelligent Material Systems and Structures 21 (5) (2010) 517–528. doi:10.1177/1045389X09359436.
URL `http://journals.sagepub.com/doi/10.1177/1045389X09359436`

[11] B. Yan, K. Wang, Z. Hu, C. Wu, X. Zhang, B. Yan, K. Wang, Z. Hu,

C. Wu, X. Zhang, Shunt Damping Vibration Control Technology: A Review, Applied Sciences 7 (5) (2017) 494. doi:10.3390/app7050494. URL http://www.mdpi.com/2076-3417/7/5/494

[12] S. Behrens, A. Fleming, S. Moheimani, Passive Vibration Control via Electromagnetic Shunt Damping, IEEE/ASME Transactions on Mechatronics 10 (1) (2005) 118–122. doi:10.1109/TMECH.2004.835341. URL http://ieeexplore.ieee.org/document/1395874/

[13] E. Turco, P. Gardonio, Sweeping shunted electro-magnetic tuneable vibration absorber: Design and implementation, Journal of Sound and Vibrationdoi:10.1016/j.jsv.2017.06.035.

[14] E. Turco, P. Gardonio, R. Petrella, L. Dal Bo, Modular vibration control unit formed by an electromagnetic proof-mass transducer and sweeping RL-shunt, Journal of Vibration and Acoustics 142 (6) (2020) 1–35. doi:10.1115/1.4047068.

[15] P. Gardonio, E. Turco, A. Kras, L. D. Bo, D. Casagrande, Semi-active vibration control unit tuned to maximise electric power dissipation, Journal of Sound and Vibration 499 (2021) 116000. doi:10.1016/J.JSV.2021.116000.

[16] A. J. Fleming, S. Behrens, S. O. Moheimani, Synthetic impedance for implementation of piezoelectric shunt-damping circuits, Electronics Letters 36 (18) (2000) 1525–1526. doi:10.1049/el:20001083.

[17] Tectonic Audio Labs, Tectonic TEAX09C005-8 Data Sheet, Tech. rep.

(2020).
URL https://www.tectonicaudiolabs.com/product/teax09c005-8/?id=product-797

[18] Dayton Audio, Dayton Audio DAEX-13-4SM Specification Sheet, Tech. rep. (2020).
URL https://www.daytonaudio.com/images/resources/295-258--dayton-audio-daex-13

[19] J. Hagedorn, F. Sell-Le Blanc, J. Fleischer, Handbook of coil winding: Technologies for efficient electrical wound products and their automated production, Springer Berlin Heidelberg, 2017. doi:10.1007/978-3-662-54402-0.

[20] M. Gendreau, J.-Y. Potvin (Eds.), Handbook of Metaheuristics, 2nd Edition, Vol. 146 of International Series in Operations Research & Management Science, Springer US, Boston, MA, 2010. doi:10.1007/978-1-4419-1665-5.
URL http://link.springer.com/10.1007/978-1-4419-1665-5

[21] O. Abdeljaber, O. Avci, D. J. Inman, Optimization of chiral lattice based metastructures for broadband vibration suppression using genetic algorithms, Journal of Sound and Vibration 369 (2016) 50–62. doi:10.1016/J.JSV.2015.11.048.
URL https://www.sciencedirect.com/science/article/pii/S0022460X16000547

[22] O. Abdeljaber, O. Avci, S. Kiranyaz, D. J. Inman, Optimization of linear zigzag insert metastructures for low-frequency vibration attenuation using genetic algorithms, Mechanical Systems and Signal

Processing 84 (2017) 625–641. doi:10.1016/J.YMSSP.2016.07.011.
URL https://www.sciencedirect.com/science/article/pii/S0888327016302382

[23] S. L. Yeh, R. L. Harne, Origins of broadband vibration attenuation empowered by optimized viscoelastic metamaterial inclusions, Journal of Sound and Vibration 458 (2019) 218–237. doi:10.1016/j.jsv.2019.06.018.

[24] L. Singleton, J. Cheer, S. Daley, Metaheuristic optimisation of an elastic metamaterial for robust vibration control, in: Proceedings of Meetings on Acoustics, Vol. 39, Acoustical Society of America, 2019, p. 045008. doi:10.1121/2.0001185.
URL http://asa.scitation.org/doi/abs/10.1121/2.0001185

[25] S. Shabir, R. Singla, A Comparative Study of Genetic Algorithm and the Particle Swarm Optimization, International Journal of Electrical Engineering 9 (2) (2016) 215–223.
URL http://www.irphouse.com

[26] S. Chen, Constrained Particle Swarm Optimization (2018).
URL https://uk.mathworks.com/matlabcentral/fileexchange/25986-constrained-par

[27] J. Kennedy, R. Eberhart, Particle Swarm Optimization, in: Proceedings of ICNN'95 - International Conference on Neural Networks, 1995, pp. 1942–1945.
URL https://ieeexplore.ieee.org/document/488968

[28] K. Deb, An efficient constraint handling method for genetic algorithms, Computer Methods in Applied Mechanics and Engineering 186 (2-4) (2000) 311–338. doi:10.1016/S0045-7825(99)00389-8.

[29] J. He, Z.-F. Fu, Modal analysis, Butterworth-Heinemann, 2001.

[30] S. Jønsson, Accurate Determination of Loudspeaker Parameters using Audio Analyzer Type 2012 and Laser Velocity Transducer Type 3544, Tech. rep., Bruel and Kjær (1996).

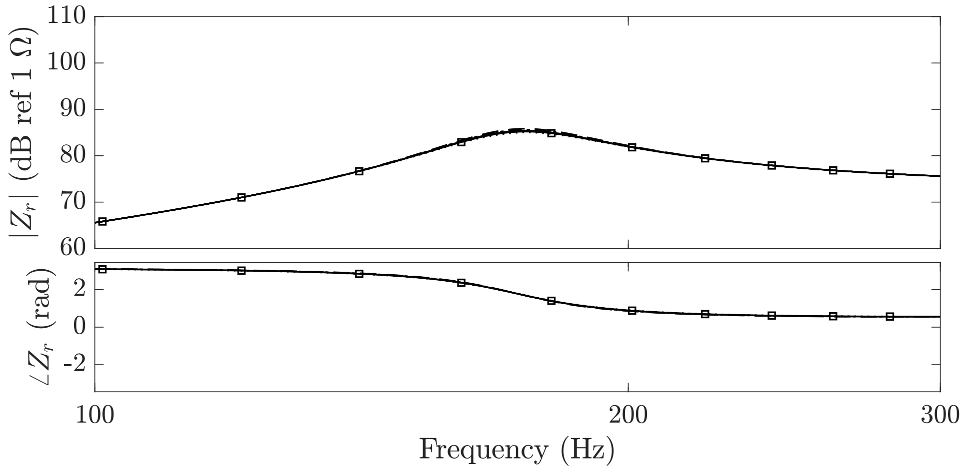

(a)

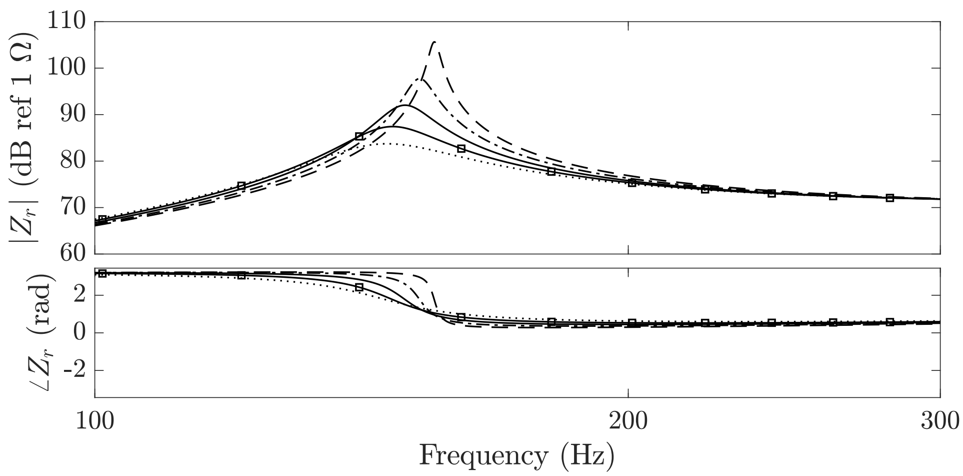

(b)

Figure 6: Impedance to displacement of the transducer base, Z_r, at different tuning frequencies ((a) f_r = 175 Hz; (b) f_r = 150 Hz) for the average value for R_e as dictated by the peak of the distribution curve, μ_{Re}, (——), and for deviation by multiples of the standard deviation of the measured distribution below (σ_1), and above (σ_2), the nominal: $\mu_{Re} - 2\sigma_1$ (– – –); $\mu_{Re} - \sigma_1$ (–·–·–); $\mu_{Re} + \sigma_2$ (—□—); $\mu_{Re} + 2\sigma_2$ (······).

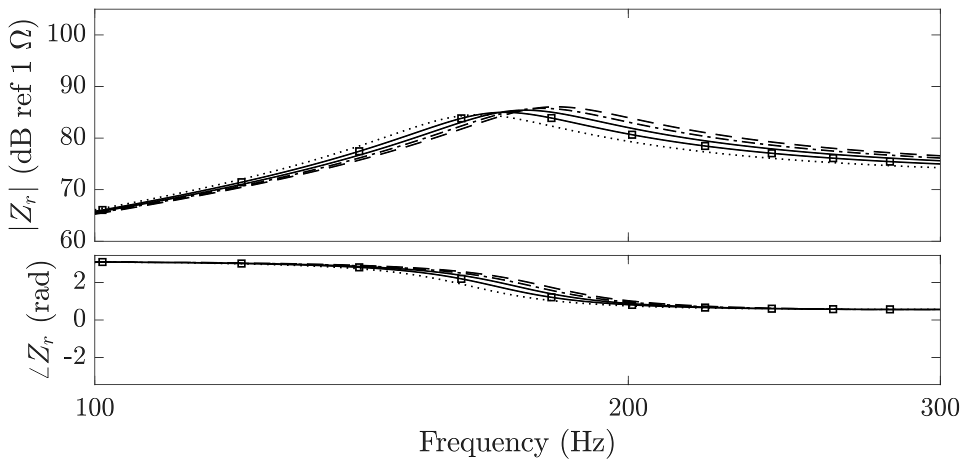

(a)

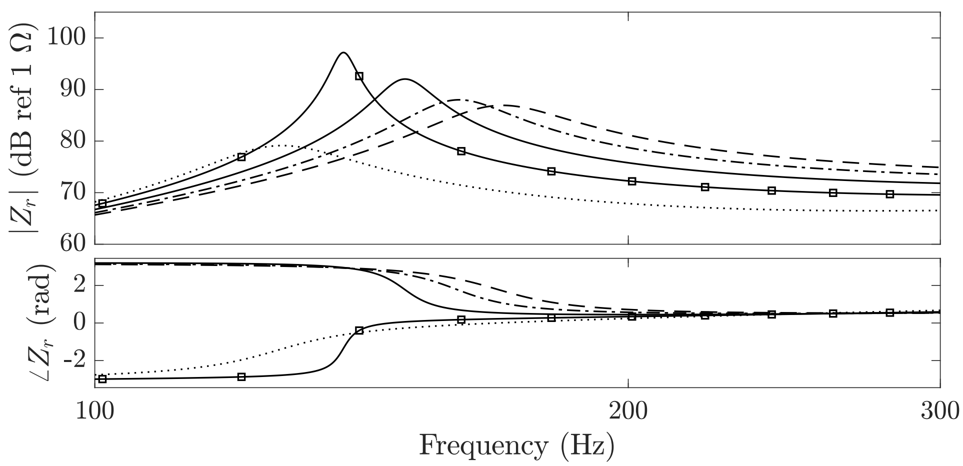

(b)

Figure 7: Impedance to displacement of the transducer base, Z_r, at different tuning frequencies ((a) $f_r = 175$ Hz; (b) $f_r = 150$ Hz) for the average value for Bl as dictated by the peak of the distribution curve, μ_{Bl}, (——), and for deviation by multiples of the standard deviation of the measured distribution: $\mu_{Bl} - 2\sigma$ (– – –); $\mu_{Bl} - \sigma$ (- - - -); $\mu_{Bl} + \sigma$ (—□—); $\mu_{Bl} + 2\sigma$ ($\cdots\cdots$).

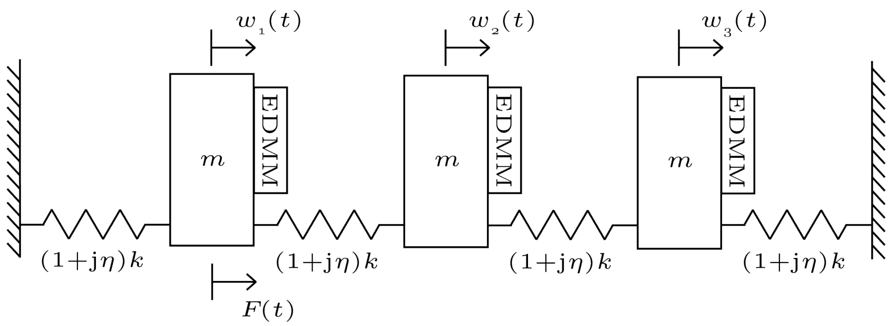

Figure 8: A diagram of the 3DOF structure used for evaluation of the optimisation procedure and EDMM response, showing the orientation and location of the EDMM, and the excitation force.

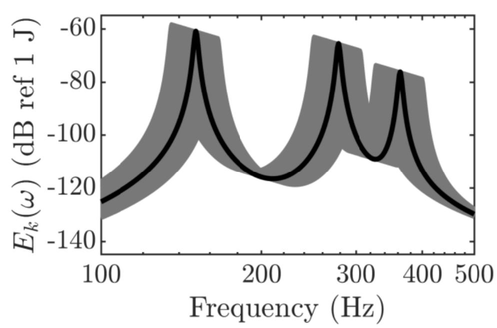

Figure 9: Total structural kinetic energy, E_k for the nominal structure (black) and the range of total structural kinetic energy for the uncertain structural responses (grey).

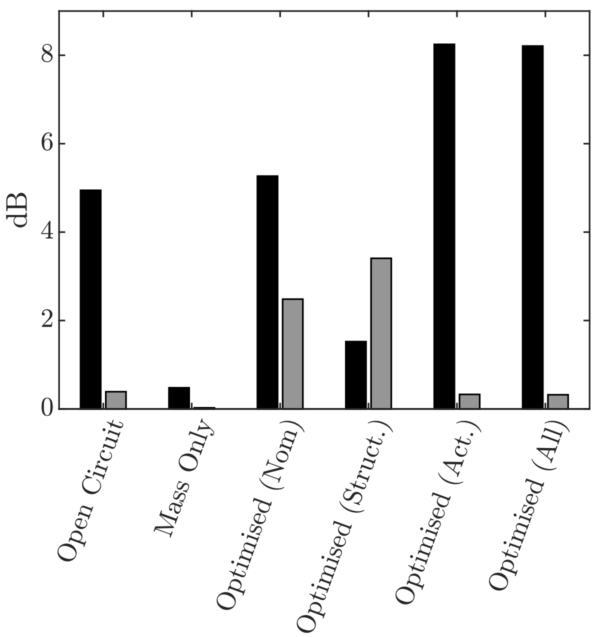

Figure 10: $\overline{E}_{k,\,atten}$ (black) and $\sigma(E_{k\ atten})$ (grey) for each considered treatment.

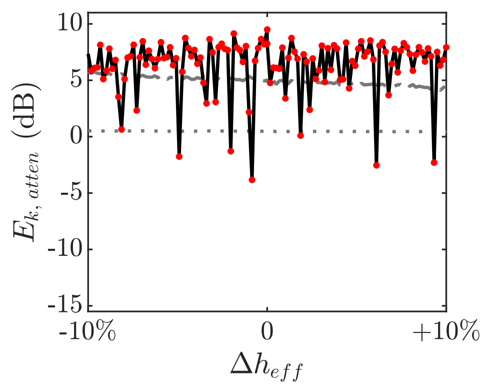

(a)

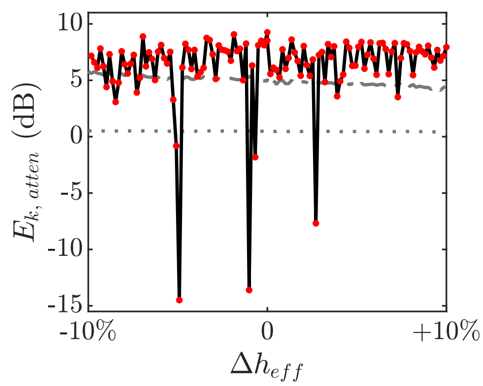

(b)

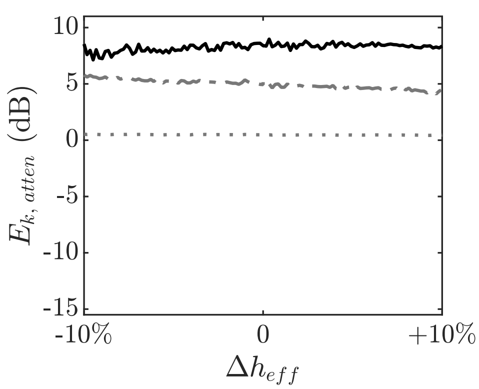

(c)

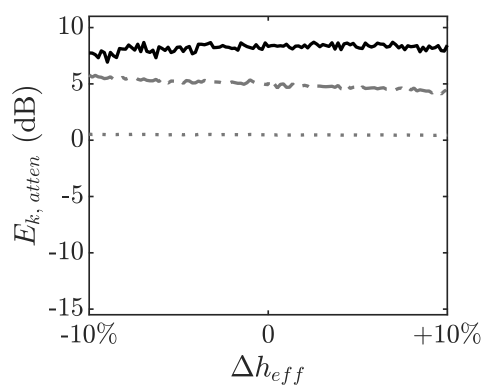

(d)

Figure 11: $E_{k,\,atten}$ achieved by the EDMM for each perturbation of the uncertain structure-EDMM model (sorted by the normalised effective thickness, Δh_{eff}). In each plot the response with the EDMM as a mass only $(\cdots\cdots)$ and the open-circuit EDMM (– – – -) are compared with the EDMM: (a) optimised for nominal performance (——); (b) optimised for robustness to uncertainty in the structure (——); (c) optimised for robustness to uncertainty in the transducers (——); (d) optimised for robustness to uncertainty in both the structure and the transducers (——). Individual cases where one or more instabilities are present in the EDMM, are highlighted in red.

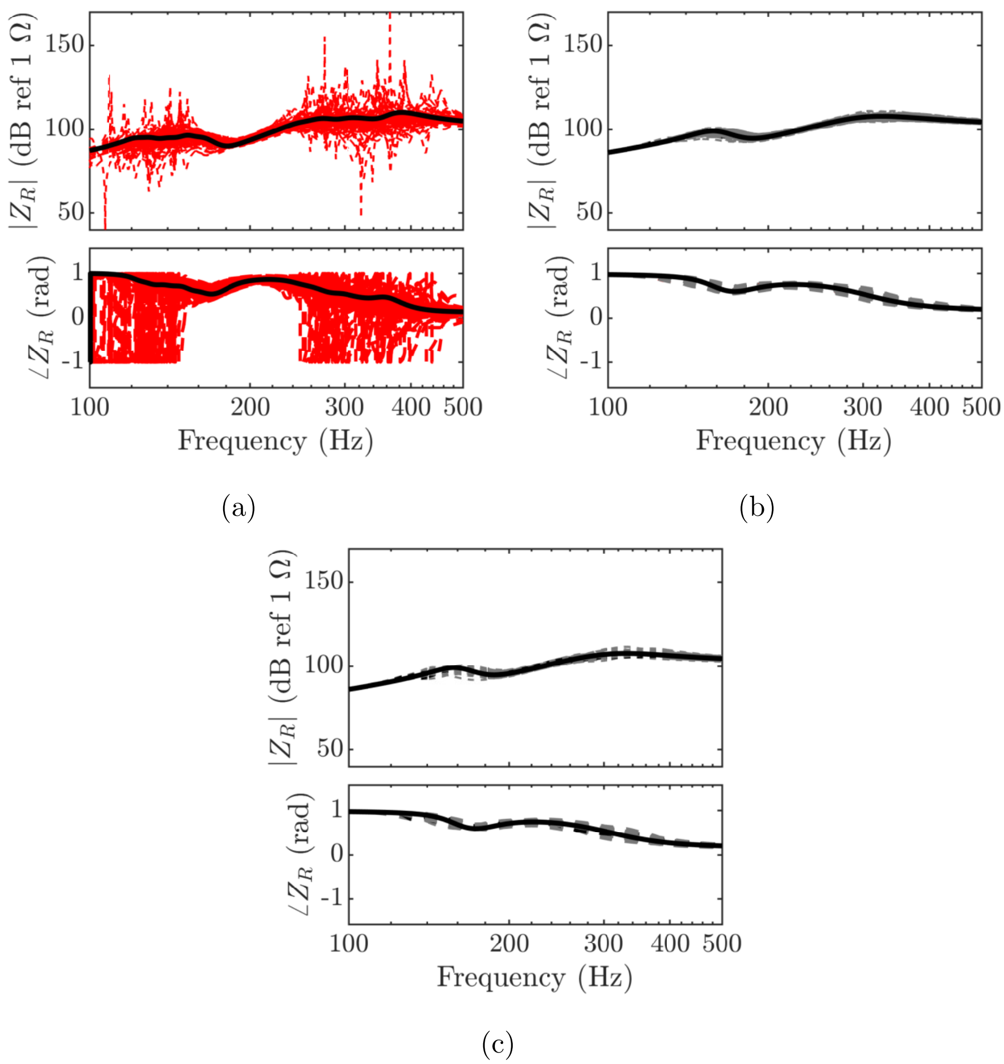

Figure 12: Resulting Zr for the nominal transducer (black, ——) and uncertain transducers (grey, – – –) when optimised for: (a) robustness with uncertainty in the structure; (b) robustness with uncertainty in the transducers; (c) robustness with uncertainty in both the structure and the transducers. Unstable responses are highlighted in red.

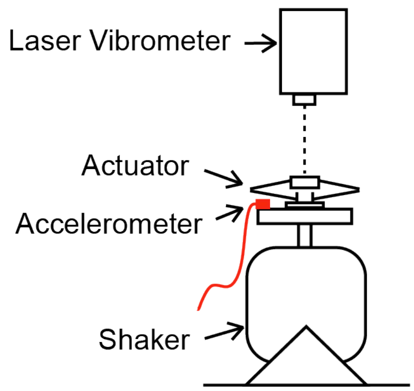

(a)

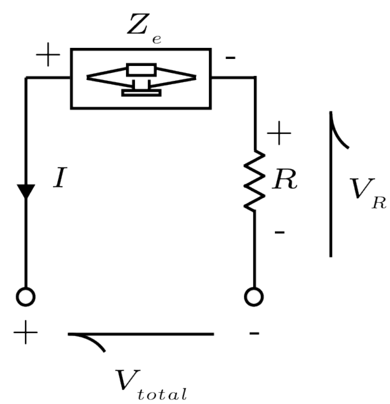

(b)

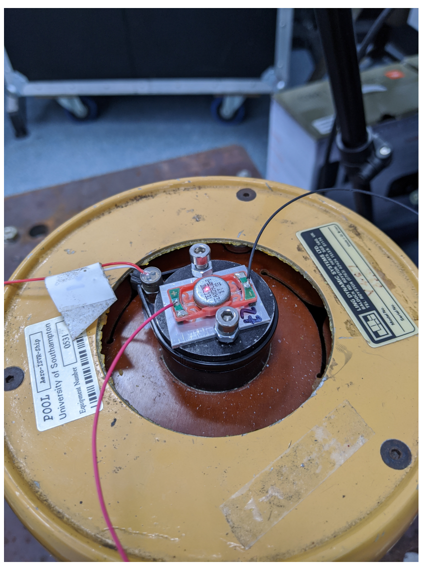

(c)

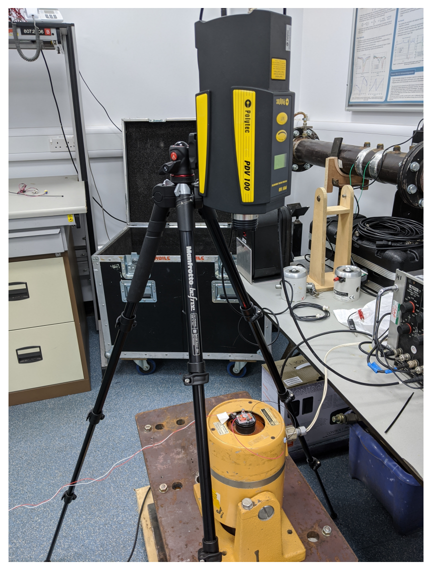

(d)

Figure A.13: Experimental measurement of transducer mechanical and electrical parameters. (a) diagram of experiment 1 - response to dynamic excitation; (b) diagram of experiment 2 - response to electrical excitation; (c) transducer mounted to shaker; (d) photo of experiment 1 setup.